Journal of Experimental Botany, Vol. 65, No. 6, pp. 1481–1496, 2014
doi:10.1093/jxb/eru024

Journal of Experimental Botany
www.jxb.oxfordjournals.org

RESEARCH PAPER

Carbon isotope discrimination during branch photosynthesis of *Fagus sylvatica*: field measurements using laser spectrometry

Lydia Gentsch[1,2,*], Patrick Sturm[1,3], Albin Hammerle[1,4], Rolf Siegwolf[5], Lisa Wingate[2], Jérôme Ogée[2], Thomas Baur[1], Peter Plüss[1], Matti Barthel[1,6], Nina Buchmann[1] and Alexander Knohl[1,7]

[1] Institute of Agricultural Sciences, ETH Zurich, Universitätsstrasse 2, 8092 Zurich, Switzerland
[2] INRA, UR1263 Ephyse, 33140 Villenave d'Ornon, France
[3] Tofwerk AG, Uttigenstrasse 22, 3600 Thun, Switzerland
[4] Institute of Ecology, University of Innsbruck, Sternwartestrasse 15, 6020 Innsbruck, Austria
[5] Laboratory for Atmospheric Chemistry/Stable Isotopes & Ecosystem Fluxes, PSI – Paul Scherrer Institute, 5232 Villigen, Switzerland
[6] Landcare Research, PO Box 40, Lincoln 7640, New Zealand
[7] Chair of Bioclimatology, Georg-August University of Göttingen, Büsgenweg 2, D-37077 Göttingen, Germany

* To whom correspondence should be addressed. E-mail: gentsch.lydia@gmail.com

Received 17 June 2013; Revised 13 December 2013; Accepted 19 December 2013

Abstract

On-line measurements of photosynthetic carbon isotope discrimination ($^{13}\Delta$) under field conditions are sparse. Hence, experimental verification of the natural variability of instantaneous $^{13}\Delta$ is scarce, although $^{13}\Delta$ is, explicitly and implicitly, used from leaf to global scales for inferring photosynthetic characteristics. This work presents the first on-line field measurements of $^{13}\Delta$ of *Fagus sylvatica* branches, at hourly resolution, using three open branch bags and a laser spectrometer for CO_2 isotopologue measurements (QCLAS-ISO). Data from two August/September field campaigns, in 2009 and 2010, in a temperate forest in Switzerland are shown. Diurnal variability of $^{13}\Delta$ was substantial, with mean diurnal amplitudes of ~9‰ and maximum diurnal amplitudes of ~20‰. The highest $^{13}\Delta$ were generally observed during early morning and late afternoon, and the lowest $^{13}\Delta$ during midday. An assessment of propagated standard deviations of $^{13}\Delta$ demonstrated that the observed diurnal variation of $^{13}\Delta$ was not a measurement artefact. Day-to-day variations of $^{13}\Delta$ were summarized with flux-weighted daily means of $^{13}\Delta$, which ranged from 15‰ to 23‰ in 2009 and from 18‰ to 29‰ in 2010, thus displaying a considerable range of 8–11‰. Generally, $^{13}\Delta$ showed the expected negative relationship with intrinsic water use efficiency. Diurnal and day-to-day variability of $^{13}\Delta$ was, however, always better predicted by that of net CO_2 assimilation, especially in 2010 when soil moisture was high and vapour pressure deficit was low. Stomatal control of leaf gas exchange, and consequently $^{13}\Delta$, could only be identified under drier conditions in 2009.

Key words: Branch bags, CO_2, *Fagus sylvatica*, laser spectrometers, leaf gas exchange, open chambers, photosynthetic carbon isotope discrimination, stem respiration.

Introduction

Photosynthetic CO_2 uptake by the terrestrial biosphere is the largest one-way flux of CO_2 out of the atmosphere (Yakir, 2003). During photosynthesis, plants preferably take up the lighter $^{12}CO_2$ isotopologue and therefore discriminate against the heavier $^{13}CO_2$ isotopologue. This process, called photosynthetic carbon isotope discrimination ($^{13}\Delta$), results in a

general ^{13}C depletion of the terrestrial biosphere compared with atmospheric CO_2 (Brugnoli and Farquhar, 2000), and is used for applications at different spatial and temporal scales. At the global scale, the substantial difference in carbon isotope discrimination between oceanic and terrestrial net CO_2 uptake has been used to constrain their relative contributions to the atmospheric CO_2 mass balance (e.g. Ciais *et al.*, 1995; Ballantyne *et al.*, 2011). At the ecosystem scale, the common isotopic disequilibrium between instantaneous photosynthesis and plant and soil respiration has been used to partition the relative contributions of photosynthesis and respiration to net ecosystem exchange (e.g. Yakir and Wang, 1996; Bowling *et al.*, 2001; Ogée *et al.*, 2003; Knohl and Buchmann, 2005; Zhang *et al.*, 2006; Zobitz *et al.*, 2008).

At the same time, $^{13}\Delta$ allows unique insights into the physiology of terrestrial plants (Cernusak *et al.*, 2013), since its variability reflects changes in photosynthetic gas exchange in response to environmental variables. For C_3 plants, $^{13}\Delta$ largely reflects the balance between CO_2 supply (conductance) and demand (carboxylation) during photosynthesis. Farquhar *et al.* (1982; recently updated by Farquhar and Cernusak, 2012) developed a model that describes how this balance determines the extent of several distinct carbon isotope discriminations during leaf CO_2 uptake, in combination with further carbon isotope discriminations during photorespiration and mitochondrial respiration. A simplified form of that model describes the two largest discrimination steps as a linear function of the ratio of CO_2 partial pressures of ambient air (c_a) and leaf intercellular air spaces (c_i):

$$^{13}\Delta = a + (\bar{b} - a)\frac{c_i}{c_a} \quad (1)$$

where a (4.4‰) is the carbon isotope discrimination during stomatal diffusion, and $\bar{b}$ (27–28‰) is the net carbon isotope discrimination during carboxylation, with the lower value generally used to account for several omitted isotope effects (for a review, see Cernusak *et al.*, 2013). If c_a is maintained constant, c_i/c_a, and thus $^{13}\Delta$, is then directly linked to the intrinsic water use efficiency of the plant, defined as the ratio of CO_2 assimilation A_n and stomatal conductance g_s, given the approximate relationship (Farquhar and Richards, 1984):

$$\frac{A_n}{g_s} \sim c_a\left(1 - \frac{c_i}{c_a}\right) \quad (2)$$

For this reason, $^{13}\Delta$ is seen as a good proxy to record changes in the leaf CO_2 supply and demand balance (Warren and Adams, 2006; Barbour *et al.*, 2011).

This mechanistic understanding of $^{13}\Delta$ and of the magnitude of involved isotope effects (see, for example, Farquhar *et al.*, 1989; Cernusak *et al.*, 2013 for a review) was largely obtained from laboratory studies under controlled conditions (e.g. Hubick and Farquhar, 1989; Barbour and Farquhar, 2000; McNevin *et al.*, 2007; Tazoe *et al.*, 2011). However, given the growing efforts to infer plant ecophysiology from atmospheric carbon isotope signals at ecosystem (Ponton *et al.*, 2006; Cai *et al.*, 2008; Riveros-Iregui *et al.*, 2011) and larger scales (Alden *et al.*, 2010; Ballantyne *et al.*, 2011), continuous gas exchange-based (on-line) field measurements of instantaneous $^{13}\Delta$ are important for quantifying the real-world variability of $^{13}\Delta$ (Harwood *et al.*, 1998; Wingate *et al.*, 2007; Bickford *et al.*, 2009, 2010; Wingate *et al.*, 2010), and for identifying its drivers in the context of the existing theoretical framework.

Measurements at the branch scale are certainly preferable in this context. Like forest canopies, branches represent mixed environments where leaves experience different microclimates (e.g. different light regimes) and where bark CO_2 cycling might impact isotopic signals of net CO_2 fluxes (Teskey *et al.*, 2008). Measurements at the branch level are hence a necessary step to scale up leaf-level $^{13}\Delta$ theories to entire forest canopies. In particular, branch-scale measurements can be useful to verify predictions from process-based ecosystem models on the sensitivity of canopy-scale $^{13}\Delta$ to gas exchange and environmental variables (Baldocchi and Bowling, 2003; Aranibar *et al.*, 2006; Chen and Chen, 2007), and also for linking canopy $^{13}\Delta$ with the carbon isotope ratios ($\delta^{13}C$) of tree biomass.

Field measurements are also needed as they enable investigations on the short- and long-term variability of $^{13}\Delta$, gas exchange, or environmental variables in natural conditions. Such investigations, as presented herein, may provide informative insights relevant for plant ecophysiological inferences from proxies of $^{13}\Delta$ at ecosystem and larger scales, such as the $\delta^{13}C$ of atmospheric CO_2 or plant organic matter (e.g. Hemming *et al.*, 2005; Lai *et al.*, 2005). Such proxies often provide useful time- and space-integrated information on the leaf CO_2 supply to demand balance, but contain no information on the importance that individual gas exchange or environmental drivers had whilst shaping this balance (Scheidegger *et al.*, 2000).

The recent development of laser spectrometers for CO_2 isotopologue measurements now allows high-frequency measurements of on-line $^{13}\Delta$, even under field conditions. However, only one field data set with several months of on-line $^{13}\Delta$ measured by laser spectrometers is currently available, for the coniferous tree species *Pinus pinaster* (Ait.) (Wingate *et al.*, 2010). To the authors' knowledge, no such data set has yet been published for a deciduous tree species. This current shortage of data sets is explained by the technical effort necessary for continuous, automated, on-line field measurements of $^{13}\Delta$ or isotopic gas exchange in general (Subke and Ineson, 2010).

This work presents continuous, hourly laser spectrometry measurements of branch $^{13}\Delta$ of three mature European beech (*Fagus sylvatica* L.) trees, carried out in a temperate mixed deciduous forest over two summer seasons. The data set was used to explore the diurnal, day-to-day, and between-year variability of on-line measured branch $^{13}\Delta$. The observed variability was quantified in terms of mean diurnal variability as well as day-to-day variability using flux-weighted daily means. Linear regression analysis helped to examine the relationship between the observed variations of $^{13}\Delta$ and environmental drivers and gas exchange variables, such as A_n, g_s, or c_i/c_a. The impact of measurement uncertainties on the observed diurnal pattern of branch $^{13}\Delta$ and the contribution of twig CO_2 efflux

to measured A_n was further evaluated. A direct comparison of the branch bag measurements to existing leaf-level $^{13}\Delta$ models such as Equation 1 is presented in a companion paper (Gentsch *et al.*, 2014).

Materials and methods

Field site and campaigns

The Lägeren research site (47°28′42.0″ N and 8°21′51.8″ E at 682 m a.s.l) is located ~20 km north-west of Zurich, Switzerland, on the south-facing slope of the Lägeren mountain (866 m a.s.l.), part of the Swiss Jura. The site is part of the Swiss air quality monitoring network NABEL, and of the international FLUXNET network (Etzold *et al.*, 2010). The vegetation is a temperate mixed-deciduous forest dominated by European beech (*F. sylvatica* L.). Mean tree height of dominant trees is ~31 m (Eugster *et al.*, 2007). Leaf unfolding starts around DOY (day of year) 115, and the vegetation period lasts between 170 and 190 d (Ahrends *et al.*, 2008). Field campaigns were conducted from 8 August to 16 September 2009 (~40 d) and from 7 August to 7 October 2010 (~60 d), and thus covered the peak and the end of the vegetation periods. Mean annual air temperature was 8.9 °C in 2009 and 7.7 °C in 2010. Annual precipitation was 774 mm in 2009 and 888 mm in 2010 (BAFU, 2010, 2011).

Field set-up

Three photosynthetic gas exchange measurement chambers (branch bags) were installed on branches of three co-dominant European beech trees, located 5–20 m apart, at ~2 m height because of the lack of a scaffolding tower. To enable measurements under conditions with full or partial exposure to direct sunlight, the branch bags were installed on branches with southern or south-eastern orientation and on trees that were situated upslope of an ~1.5 ha large windthrow area. The branch bags were installed on exactly the same branches during both campaigns. The heights of the selected trees were 17–20 m and the diameter at breast height ranged from 165 mm to 260 mm.

The three branch bags were part of a larger chamber measurement set-up that also included three stem chambers and nine soil chambers that were connected via a custom-made valve switching system to a laser spectrometer for CO_2 isotopologue measurements (QCLAS-ISO, Aerodyne Research Inc., Billerica, MA, USA) and a laser spectrometer for water vapour isotopologue measurements (WVIA, Los Gatos Research Inc., Mountain View, CA, USA). The laser spectrometers were located in an air-conditioned hut. CO_2 isotope ratios and concentration were measured continuously at 1 Hz by the QCLAS-ISO instrument. The basic measurement principle of the QCLAS-ISO is an absorption-based quantification of the three main CO_2 isotopologues, $^{12}C^{16}O_2$, $^{13}C^{16}O_2$, and $^{12}C^{16}O^{18}O$, using a quantum cascade laser operating at a wavelength near 4.3 µm (2310 cm^{-1}). Specific information on the instrument set-up and design can be found in Sturm *et al.* (2012), Nelson *et al.* (2008), and Tuzson *et al.* (2008). From the WVIA, only the water vapour concentration measurements were used. Details on the WVIA instrument set-up can be found in Sturm and Knohl (2010). During the 2009 campaign, all chambers were measured within 60 min. For the 2010 campaign, a 90 min measurement sequence was adapted, with branch bags being measured twice during each sequence (every 45 min). A 6 min calibration routine (see the Supplementary data available at *JXB* online) was conducted after each measurement sequence. Characterization of reference gases was expressed on the WMO scale for CO_2 and on the V-PDB-CO_2 scale for isotope ratios (Kaiser, 2008). Long-term stability for calibrated measurements of CO_2 concentrations, $\delta^{13}C$, and $\delta^{18}O$ were ±0.30 ppm, ±0.19‰, and ±0.31‰, respectively, during the 2009 campaign, and ±0.22 ppm, ±0.21‰, and ±0.21‰ during the 2010 campaign.

Full automation of the measurement system was accomplished with ICPCON modules (I-7000 series, ICP DAS Co., Hukou Township, Taiwan), providing the means for network communication, data acquisition, and system control. The ICPCON modules were remotely controlled by a customized LabVIEW program (National Instruments Corp., Austin, TX, USA). Three-way solenoid valves (VKF300 and VDW series, SMC Pneumatik AG, Weisslingen, Switzerland) allowed constant flushing of the chamber sampling tubes. For the 2009 campaign, PTFE tubing (4 mm inner diameter; Serto AG, Aadorf, Switzerland) was used and connected with brass fittings (Swagelok by Arbor Ventil and Fitting AG, Niederrohrdorf, Switzerland). For the 2010 campaign, all tubing associated with branch bag air streams was replaced with heated PTFE tubing (0.25 inch inner diameter; TEF1H06, Indunorm Hydraulik GmbH, Duisburg, Germany). For heating the tubes, a stainless steel mesh, sheathing the inner PTFE core, was supplied with an electric current, providing a temperature increase of ~15 °C above ambient temperature inside the PTFE tube. Electrical insulation was provided by additional plastic coatings. In addition, the valve switching system, placed in four weatherproof enclosures, was also heated using heating tape (HST 42 to 250°, Horst GmbH, Lorsch, Germany), regulated by a miniature temperature controller (CT325-PD2C1, Minco EC AG, Wil, Switzerland). The longest tubing distance from a branch bag to the laser spectrometers was 76 m. Volume flow rate through the tubing was 1.45 dm^3 min^{-1}.

Branch bag operating principle

The custom-built branch bags were designed as steady-state through-flow (open dynamic) chambers (Pumpanen *et al.*, 2004). The branch bags (Fig. 1) consisted of two 10 mm thick ellipsoid (550 mm major axis, 200 mm minor axis) plexiglass end pieces, connected by four 800 mm long aluminium rods. This inner frame was covered with a highly transparent, custom-made sleeve (PTFE-Spezialvertrieb GmbH, Stuhr, Germany), made from 50 µm thin FEP-film (Norton® FEP-WF, Saint-Gobain, Willich, Germany). The FEP-sleeve was clamped between a foamed rubber layer covering the plexiglass end pieces and a tightened thin steel rope. The resulting total branch bag volume was 69 dm^3 and enclosed 110–250 leaves. Total leaf area for each branch bag was determined after both field campaigns using a leaf area meter (LI-3000A and LI-3050A; LI-COR Biosciences, Lincoln, NE, USA). Embedded in both plexiglass end pieces were axial fans (4484F, ebm-papst AG, Oberhasli, Switzerland), used for flushing the branch bag air volume between measurements by blowing air unidirectionally at a high flow rate (2833 dm^3 min^{-1}) through the branch bag. The fans were covered with flaps, which were moved by electric motors (VMC 24 V 0,26 W, Robert Bosch GmbH, Karlsruhe, Germany). Each branch bag was equipped with a PAR (photosynthetic active radiation) sensor (SQ-110, Apogee Instruments Inc., Logan, UT, USA), mounted outside the respective branch bag. Air temperature and relative humidity inside the branch bag were measured with a combined sensor (HygroClip S3-C03, Rotronic AG, Bassersdorf, Switzerland). Leaf temperature was measured with two thermocouples (PTFE-coated Thermocouple Type T 0.08 mm, Omega Engineering Inc., Stamford, CT, USA), attached to the lower sides of two leaves. Two branch bags were equipped with additional thermocouples (Thermocouple Type T 0.2 mm, TC-Direct, Mönchengladbach, Germany) for duplicate air temperature measurements. Branch bags were fixed to a flexible rope attached to the respective tree trunk and a wooden pole.

Thirty minutes before the start of each measurement, the flushing fans were switched off and flaps were closed. Next, a blowing axial fan (D481T-024KA-3, Micronel AG, Tagelswangen, Switzerland) was set to a defined flow rate (daytime range: 9–60 dm^3 min^{-1}), producing a constant flow of air through the branch bag, necessary for establishing steady-state conditions. The flow rate through the chamber was set depending on incoming PAR at the time of flap closure and monitored by an air mass flow sensor (AWM 720P1, Honeywell Sensing and Control, Golden Valley, MN, USA).

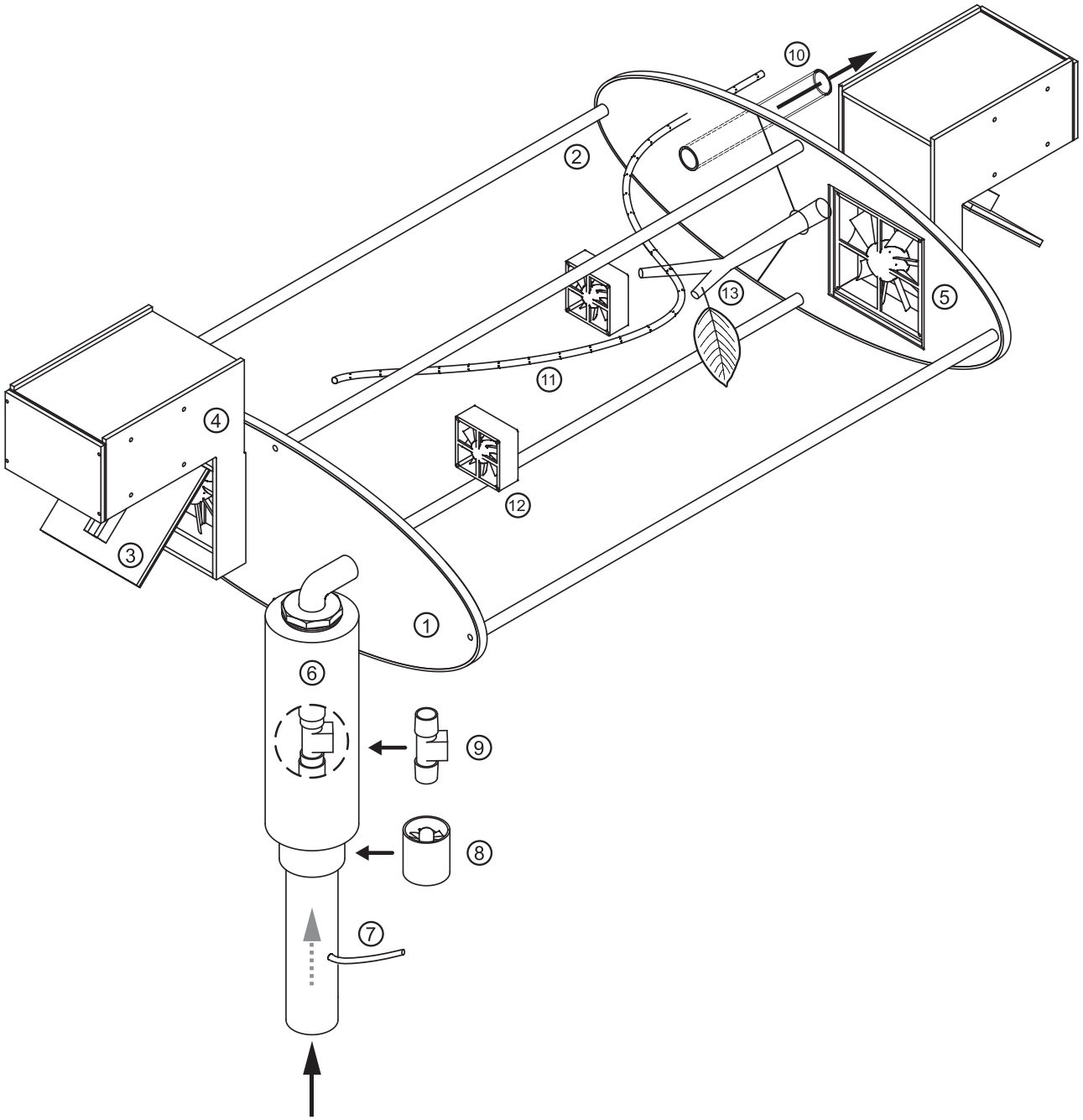

Fig. 1. Schematic of the branch bag used in this study: (1) plexiglass end piece, (2) aluminium rod, (3) flap covering the flushing fan, (4) electric motor, (5) flushing fan, (6) chamber inlet unit, (7) sample tube for inlet (ambient) air, (8) blowing axial fan, (9) mass flow meter, (10) chamber outlet tube, (11) sample tube for chamber air, (12) mixing fan, and (13) branch. The FEP film covering the construction is not shown.

A minimum daytime flow rate of 9 dm^3 min^{-1} was imposed to ensure the establishment of steady-state conditions within 30 min (Rayment, 2000). Flow rate constancy was ensured by a LabVIEW-mediated feedback control of an ICPCON analogue output module (I-7024-CR, ICP DAS Co., Hukou Township, Taiwan) and a pulse width modulator (K8004, Velleman Components NV, Gavere, Belgium). The blowing axial fan and the air mass flow sensor were connected to a 20 mm wide PVC inlet tube, mounted on one of the plexiglass end pieces. The PVC inlet tube was further connected to a 100 dm^3 buffering volume (PE-barrel OFF-100, Faserplast AG, Rickenback, Switzerland) via PVC tubing (inner diameter 25 mm; Cristallo Extra AL, Fitt S.p.A., Sandrigo, Italy), drawing in air at a height of 2 m. Air exited the branch bag through an outlet tube (20 mm inner diameter, 450 mm length) attached to the opposite plexiglass end piece. Inside the branch bags, two additional axial fans (450 dm^3 min^{-1}; D06T24LWS, Traco Industrietechnik AG, Zurich, Switzerland) ensured adequate mixing of the air volume enclosed. The choice of the FEP foil and the approach to flow rate establishment were inspired by a grassland chamber system presented in Pape *et al.* (2009). The PAR-dependent flow rate regulation was primarily necessary to maintain daytime CO_2 concentration drawdowns (c_e–c_o) in a range that ensured sufficient differences in the carbon isotope ratios of air outside and inside the branch bags (δ_e–δ_o), a prerequisite for keeping the error of $^{13}\Delta$ small. A $|\delta_e–\delta_o| > 2‰$ was achieved for 80% of all cases, which was 10 times larger than the QCLAS-ISO instrument precision.

Sampling air flow was 1.45 dm^3 min^{-1} and entirely independent of the air flow used to establish the steady state. Ambient air (inlet

measurement providing c_e and δ_e values) was sampled at the branch bag inlet, after the buffering volume and before the mass flow sensor. Branch bag air (outlet measurement providing c_o and δ_o values) was sampled with a perforated PTFE tube, extending over the branch bag length. A single branch bag measurement consisted of two inlet measurements (lasting 55 s in 2009 and 80 s in 2010) and one outlet measurement (lasting 105 s in 2009 and 110 s in 2010), with the inlet measurements carried out before and after the respective outlet measurement. The 1 Hz laser spectrometry measurements were averaged to a 5 s logging interval, resulting in at least 22 inlet and 21 outlet values per each branch bag measurement.

Twig CO_2 efflux measurements

The magnitude of CO_2 efflux from the woody material enclosed in the branch bags (twig CO_2 efflux) was estimated with two different methods that are described in detail in the Supplementary data available at *JXB* online. First, custom-made twig chambers enabled individual measurements of twig CO_2 efflux under full light or darkened conditions that were carried out during six campaigns in 2010. Secondly, a 5 d continuation of adjusted branch bag measurements after the leaf harvest on 7 October 2010 enabled continuous observations of diel dynamics of twig CO_2 efflux.

Calculation of $^{13}\Delta$, error propagation, and data handling

The on-line measured photosynthetic carbon isotope discrimination of whole branches, $^{13}\Delta$, was calculated following Evans *et al.* (1986), from QCLAS-ISO measured concentrations and carbon isotope compositions of CO_2 in air entering (c_e, δ_e) and leaving (c_o, δ_o) the branch bag at steady-state conditions:

$$^{13}\Delta = \frac{\xi(\delta_o - \delta_e)}{1 + \delta_o - \xi(\delta_o - \delta_e)} \quad \textbf{with} \quad \xi = \frac{c_e}{c_e - c_o} \tag{3}$$

Standard deviations (SDs) of δ_e, δ_o, c_e, and c_o were propagated into the SD of $^{13}\Delta$ (SD_{BB}), according to Gaussian error propagation rules (Taylor, 1997). An analysis of $^{13}\Delta$ derivatives and the correlation between the SDs of measurement means of c_e and δ_e, as well as c_o and δ_o, indicated the true SD of $^{13}\Delta$ to be smaller than calculated with the Gaussian error propagation method. The fraction of SD_{BB} deriving solely from QCLAS-ISO instrument precision (SD_{LS}) was approximated analogously to SD_{BB}, but using the above-stated QCLAS-ISO long-term instrument stability of CO_2 and $\delta^{13}C$ measurements in 2010 as values for c_e, c_o, δ_e and δ_o, respectively. $^{13}\Delta$ was only calculated if corresponding PAR was >10 µmol m^{-2} s^{-1}. Measurements with a high inlet or outlet variability (c_e–c_o) <10 ppm or a propagated SD of $^{13}\Delta$ >6‰ were discarded. Generally, all measured and calculated variables denoted with 'daily' (subscript X_D) refer to times of the day with PAR >10 µmol m^{-2} s^{-1}. Data processing and statistical analysis were done using R 2.9.2 (R Development Core Team, 2009) and MATLAB (The MathWorks Inc., Natick, MA, USA). All equations used for calculating gas exchange and environmental variables as well as the definition for $^{13}\Delta$, $\delta^{13}C$, and the calculation of daily variables are given in the Supplementary data available at *JXB* online.

Results

Diurnal patterns in branch microclimate, gas exchange, and $^{13}\Delta$

Mean diurnal trends in branch microclimate, gas exchange, and $^{13}\Delta$, observed during the 2010 campaign, are summarized in Fig. 2. Mean diurnal patterns of incident PAR differed among the three different branch bags (Fig. 2A, B). Branch bags one (BB1) and three (BB3) received high PAR rates only for 2–3 hours per day, while the location of branch bag two (BB2) next to a forest glade resulted in a noticeably broader PAR peak. Mean diurnal variations of air temperature (T_{air}) and air vapour pressure deficit (VPD) within the branch bags generally tracked variations in PAR (Fig. 2C–F). Mean diurnal patterns of branch microclimate were strongly reflected by those of net CO_2 assimilation (A_n; Fig. 2I, J), but less by those of stomatal conductance to CO_2 (g_s; Fig. 2G, H). BB2 generally displayed greater A_n and g_s (Fig. 2; Table 2) and a smaller average leaf width than the other two branch bags (36 mm versus 42 mm and 39 mm for BB1 and BB3, respectively; data only collected in 2010), indicating a stronger sun adaptation of leaves of BB2 compared with those of BB1 and BB3. Mean diurnal variations of $^{13}\Delta$ (Fig. 2K, L) were substantial and strongly tracked mean diurnal variations in A_n (Fig. 2I–L). The highest $^{13}\Delta$ were generally observed during early morning and late afternoon, while the lowest $^{13}\Delta$ were generally observed during midday (Table 2). Mean diurnal amplitudes of $^{13}\Delta$ were ~10‰ (2009, ~9‰; 2010, ~11‰) on days classified as sunny and ~6‰ (2009, ~5‰; 2010, ~7‰) on days classified as cloudy (Fig. 2K, L). The mean diurnal pattern of $^{13}\Delta$ was thus persistent for both sunny and cloudy days, despite the considerably smaller mean diurnal variation of potential driving variables on cloudy days (Fig. 2A–H). The observed maximum diurnal amplitudes in 2009 and 2010 were 17‰ and 23‰, respectively. BB2 generally displayed lower mean $^{13}\Delta$ than BB3 and BB1 (Fig. 2K, L). Bulk leaf material sampled from the BB2 measurement tree likewise exhibited higher $\delta^{13}C$ values than that sampled from the BB1 and BB3 measurement trees (Table 3). Although there was a distinct and persistent diurnal $^{13}\Delta$ pattern, short-term variability of $^{13}\Delta$ could be considerable for two consecutive measurements (every 45–60 min), depending on the variability of weather conditions at the field site (data not shown).

The propagated standard deviation of $^{13}\Delta$ (SD_{BB}) was used to assess diurnal signal-to-noise ratios (Fig. 3). As expected for open chambers under steady-state conditions, SD_{BB} decreased with higher CO_2 drawdown between inlet (c_e) and outlet air (c_o), usually occurring at midday. In general, SD_{BB} tended to be higher for BB2 than for the other two branch bags. This was caused by a higher variability of the BB2 inlet measurements (δ_e and c_e). The uncertainty of open chamber-measured $^{13}\Delta$ has been shown to be linearly related to $\xi = c_e/[c_e - c_o]$ (Evans *et al.*, 1986; von Caemmerer and Evans, 1991), and diurnal patterns of ξ are displayed in the right panel of Fig. 3. Dark grey areas in the left panel of Fig. 3 represent the mean SD_{BB} associated with the mean $^{13}\Delta$ for all days of the 2010 campaign (52 d with data) at a certain hour of the day. Mean SD_{BB} was <2‰ for measurements conducted from 9:00 to 16:00 h Central European Time (CET) and <3.5‰ for early morning and late afternoon measurements. The fraction of SD_{BB} originating solely from QCLAS-ISO instrument precision (SD_{LS}; inner light grey areas) ranged between 24% and 56% of SD_{BB}, and was largest at small c_e–c_o, for example during early morning and late afternoon hours. The overall magnitudes of mean $^{13}\Delta$ and mean SD_{BB} clearly demonstrated

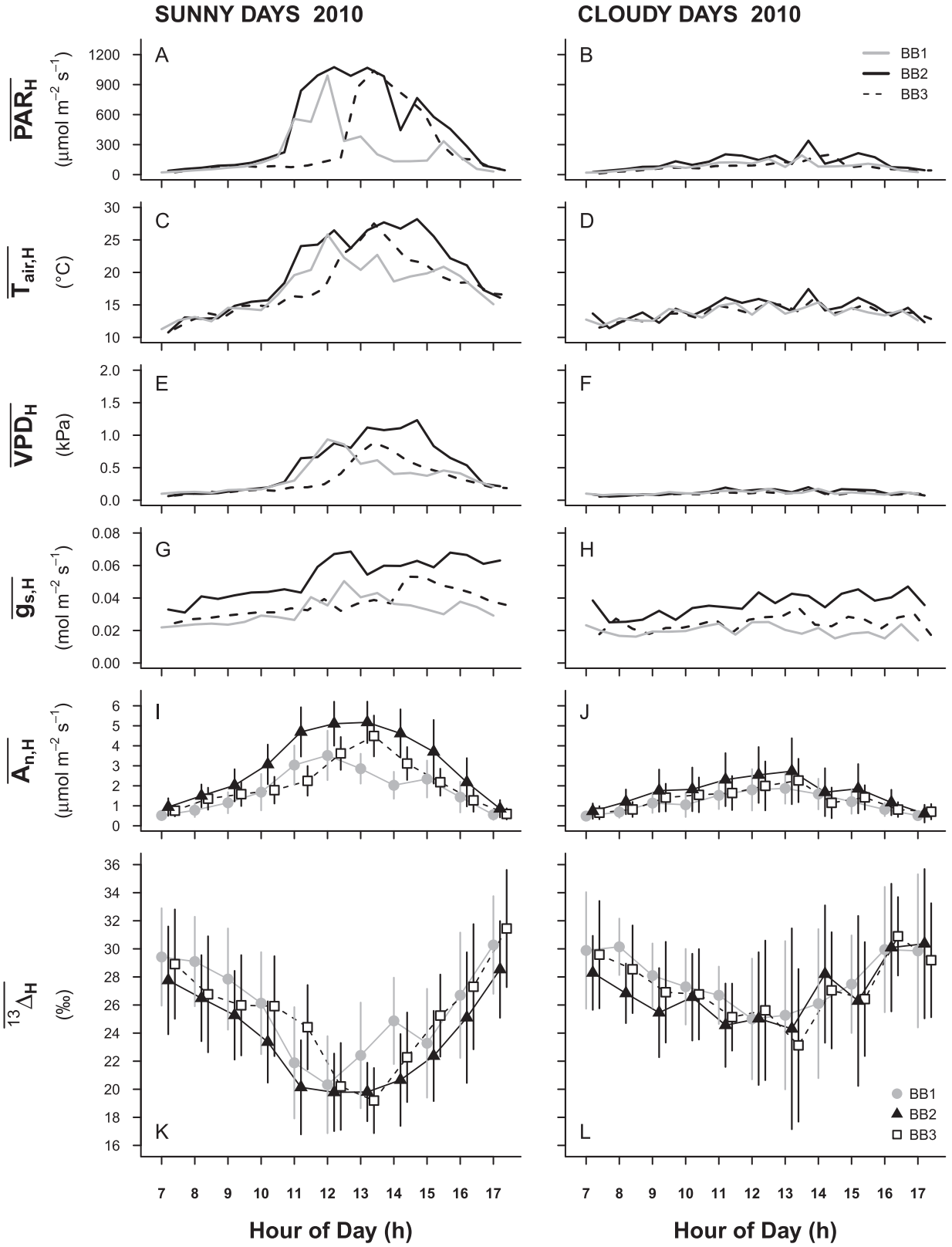

Fig. 2. Mean diurnal time courses of branch microclimate, gas exchange, and photosynthetic ^{13}C discrimination for 42 sunny days (mean midday PAR >300 µmol m^{-2} s^{-1}) and 11 cloudy days (mean midday PAR <300 µmol m^{-2} s^{-1}) during the 2010 campaign. Different symbols and lines are used to differentiate measurements from three branch bags. (A, B) Photosynthetic active radiation; (C, D) air temperature inside the branch bags; (E, F) air vapour pressure deficit inside the branch bags; (G, H) stomatal conductance for CO_2; (I, J) net CO_2 assimilation; (K, L) photosynthetic ^{13}C discrimination. Error bars indicate ±1 SD and represent day-to-day variations.

Table 1. *Abbreviations used in the text*

Abbreviation	Definition	Unit
A_n	Measured rate of branch net CO_2 assimilation per unit leaf area	μmol m^{-2} s^{-1}
$A_{n,D}$	Cumulated daily A_n	mmol m^{-2} d^{-1}
BB1 to BB3	Branch bag number one to three	–
a	^{13}C fractionations during CO_2 diffusion through the stomata (4.4‰)	‰
$\bar{b}$	Net ^{13}C discrimination during carboxylations in C_3 plants in $^{13}\Delta_{simple}$, adjusted to account for omitted CO_2 transfer resistances	‰
c_a=c_o	CO_2 mole fraction in branch bag air	μmol mol^{-1}
c_e	CO_2 mole fraction in ambient air outside the branch bags	μmol mol^{-1}
c_i	CO_2 mole fraction in leaf intercellular air spaces	μmol mol^{-1}
δ_e	Carbon isotope ratio of ambient air outside the branch bags	‰
δ_o	Carbon isotope ratio of branch bag air	‰
$^{13}\Delta$	Observed net ^{13}C discrimination during branch photosynthesis (Equation 3)	‰
$\overline{^{13}\Delta_H}$	Hourly means of $^{13}\Delta$ over all days of a respective field campaign (2009 or 2010). Hours relate to the subsequent hour (CET)	‰
$\overline{^{13}\Delta_D}$	Flux-weighted daily arithmetic means of $^{13}\Delta$	‰
$\delta^{13}C_{air}$	$\delta^{13}C$ of ambient air, measured at branch bag inlets during the day (PAR >10 μmol m^{-2} s^{-1})	‰
$\delta^{13}C_{as}$	$\delta^{13}C$ of recent assimilates, calculated from $^{13}\Delta$ and $\delta^{13}C_{air}$	‰
$\overline{\delta^{13}C_{as,D}}$	Flux-weighted daily arithmetic mean of the $\delta^{13}C_{as}$	‰
$\delta^{13}C_{bulk}$	$\delta^{13}C$ of leaf bulk organic matter, sampled outside the branch bags, but from the same tree	‰
E	Measured rate of branch transpiration per unit leaf area	mol m^{-2} s^{-1}
g_s	Observed stomatal conductance to CO_2 for the entire leafy branch	mol m^{-2} s^{-1}
A_n/g_s	Intrinsic water use efficiency	μmol mol^{-1}
PAR	Measured photosynthetic active radiation	μmol m^{-2} s^{-1}
PAR_D	Cumulated daily PAR	μmol m^{-2} d^{-1}
SD_{BB}	One propagated standard deviation for each $^{13}\Delta$ measurement.	‰
SD_{LS}	One propagated standard deviation of $^{13}\Delta$, assuming that standard deviations for δ_e, δ_o, c_e, and c_o equal the long-term stability of the QCLAS-ISO instrument for CO_2 and $\delta^{13}C$ measurements given in the Materials and methods	‰
$\overline{SD_{BB,H}}$	Hourly means of all SD_{BB} over all days of the 2010 campaign	‰
$\overline{SD_{LS,H}}$	Hourly mean of all SD_{LS} over all days of the 2010 campaign	‰
T_{air}	Air temperature (figure legends state if inside or outside the branch bags)	°C
VPD	Air vapour pressure deficit (figure legends state if inside or outside the branch bags)	kPa
$\overline{X_H}$	Hourly means of any variable X over all days of a field campaign (2009 or 2010). Denotes both hourly and half-hourly means, see definition in figure legends. Hours always relate to the subsequent hour (CET)	–
$\overline{X_D}$	Simple daily means of any variable X, if not defined as flux-weighted daily means; daily always includes daytime measurements only	–
$\overline{X_C}$	Campaign means for 2009 or 2010 of any variable X (see definition if flux-weighted or not)	–

Table 2. *Hourly means±1SD for A_n (μmol m^{-2} s^{-1}) and $^{13}\Delta$ (‰) of three branch bags (BB1–BB3) during all days of the 2009 and 2010 campaigns*

Data are given for 7:00–8:00 (7), 12:00–13:00 (12), and 17:00–18:00 h (17) CET.

	7 CET mean±SD_H		12 CET mean±SD_H		17 CET mean±SD_H	
	2009	**2010**	**2009**	**2010**	**2009**	**2010**
A_n						
BB1	0.6±0.2	0.5±0.2	3.7±1.3	3.1±1.4	0.8±0.3	0.6±0.2
BB2	1.5±0.7	0.9±0.4	4.0±1.6	4.5±1.6	1.2±0.5	0.8±0.4
BB3	1.1±0.6	0.7±0.3	3.3±1.2	3.3±1.1	0.7±0.4	0.6±0.3
$^{13}\Delta$						
BB1	25.0±1.6	29.5±3.5	18.7±3.7	21.4±4.1	25.1±2.4	30.2±3.8
BB2	21.5±2.1	27.9±3.6	17.2±3.5	21.0±4.0	21.7±2.8	28.9±3.9
BB3	22.3±2.9	29.0±3.9	17.3±3.0	21.3±4.1	22.5±3.8	31.1±4.2

Table 3. *Campaign means ±1 SD of $\delta^{13}C$ of daytime inlet (ambient) air, flux-weighted daily mean of $^{13}\Delta$, $\delta^{13}C$ of assimilates calculated using equation A18 of the Supplementary data available at JXB online for all branch bags (BB1–BB3), and $\delta^{13}C$ of bulk leaf material, sampled outside the branch bags, but from the same tree*

All numbers are given in ‰. n=34 and 50 measurement days in 2009 and 2010, respectively, except for $\overline{\Phi^{13}C_{bulk,C}}$ with n=12 and 11 samplings days in 2009 and 2010, respectively.

	$\overline{\delta^{13}C_{as,C}}$ ±SD$_C$	$\overline{\delta^{13}C_{bulk,C}}$ ±SD$_C$	$\overline{^{13}\Delta_C}$ ±SD$_C$	$\overline{\Phi^{13}C_{bulk,C}}$ ±SD$_C$
2009				
BB1	–8.9±0.4	19.4±1.5	–28.7±1.6	–31.4±0.5
BB2	–8.9±0.4	18.5±1.7	–27.7±1.9	–30.4±0.4
BB3	–9.0±0.5	19.1±2.0	–28.5±2.3	–32.1±0.3
2010				
BB1	–9.4±0.5	23.5±2.4	–33.5±2.7	–31.8±0.4
BB2	–9.4±0.5	21.9±2.3	–31.8±2.6	–29.8±0.4
BB3	–9.5±0.5	23.1±2.2	–33.1±2.4	–31.2±0.4

that observed mean diurnal variations of $^{13}\Delta$ were real and not a measurement artefact.

Twig CO_2 efflux, measured with either the twig chamber or the branch bag method, was always <0.8 µmol m^{-2} s^{-1}, when referenced to the bark surface area (Table 4). The continuous branch bag method revealed a diel time course of twig CO_2 efflux, with typical night-time values of ~0.4 µmol m^{-2} s^{-1}, reducing throughout the morning to an eventual midday reduction of <0.1 µmol m^{-2} s^{-1}. The twig chamber method likewise showed generally higher twig CO_2 efflux under dark than under light conditions (in 27 out of 33 measurement pairs). In half the cases, light values were reduced by >40% relative to the dark values. The ratio of bark surface area to leaf surface area ranged from 0.06 to 0.12 for the branches enclosed in the three branch bags (Table 4). Considering the largest ratio of 0.12 and the highest observed twig CO_2 efflux of 0.8 µmol m^{-2} s^{-1}, the maximum contribution of twig CO_2 efflux to A_n was estimated to be <0.1 µmol m^{-2} s^{-1}.

Day-to-day trends in environmental and gas exchange variables and $^{13}\Delta$

The two field campaigns were characterized by distinct differences in their weather regime. Frequent rain events during the 2010 campaign led to ~10 vol% higher soil moisture at 5 cm depth in 2010 than in 2009 (Fig. 4E). While air temperatures were comparable for both campaigns (see Supplementary Fig. S5 available at *JXB* online), VPD were commonly higher in 2009 than in 2010 (Fig. 4D), except for the more shaded BB1. Flux-weighted daily means of $^{13}\Delta$ ($\overline{^{13}\Delta_D}$; Fig. 4A) displayed pronounced day-to-day changes, with values ranging from 15‰ to 23‰ in 2009 and from 18‰ to 29‰ in 2010. Temporal $\overline{^{13}\Delta_D}$ variability over each campaign was two to three times larger than the spatial $\overline{^{13}\Delta_D}$ variability between trees (temporal, SD of $\overline{^{13}\Delta_D}$ over all days=2.1‰ in 2009 and 3.1‰ in 2010; spatial, daily SD of $\overline{^{13}\Delta_D}$ over the three trees=1.0‰ for both years). Values were ~3‰ lower in 2009 compared with 2010, even when considering the same time period (DOY 220 to DOY 258) during both years (Fig. 4A). This difference was also reflected in the minimum and maximum daily values of $^{13}\Delta$ (9‰ and 32‰ in 2009 and 13‰ and 41‰ in 2010). The most noticeable feature during the 2009 field campaign was a steady decline of $^{13}\Delta$ in August (Fig. 4A), co-occurring with a steep decline of soil moisture, that was only slightly suspended by smaller rain events between DOY 233 and DOY 237 (Fig. 4E). Mean daily g_s likewise showed a steady decline during that time period (Fig. 4C), that was even less pronounced for BB1. Cumulated daily A_n declined concurrently but recovered swiftly during DOY 234 and DOY 235 (Fig. 4B). In contrast, an increasing trend for $^{13}\Delta$ was observed during the 2010 field campaign (Fig. 4A).

Indications on drivers of $^{13}\Delta$ variability from linear regression analysis

Linear regression analysis was used to quantify the predictive power of gas exchange and environmental variables for the observed variability of $^{13}\Delta$, in order to obtain indications about its dominant drivers under varying environmental conditions, or in terms of CO_2 supply and demand balance. Figure 5 shows regressions of individual measurements of $^{13}\Delta$ with A_n, g_s, or c_i/c_a. Figure 6 shows regressions of flux-weighted daily means of $^{13}\Delta$ and daily gas exchange and environmental variables, allowing a shift of focus towards potential drivers of the day-to-day variability of $^{13}\Delta$ (Fig. 4).

Individual measurements of $^{13}\Delta$ displayed a strong negative linear relationship with those of A_n (Fig. 5, left panels), in particular during the 2010 field campaign (2009, r^2>0.24; 2010, r^2>0.64). A dominating influence of A_n variability on $^{13}\Delta$ variability was further supported by a curvilinear relationship between individual measurements of $^{13}\Delta$ and PAR that resembled inverted light response curves of A_n (Supplementary Fig. S1 available at *JXB* online). These regressions of $^{13}\Delta$ with A_n and PAR supported the idea that the high diurnal variability of $^{13}\Delta$ was likely to reflect a dominating role of A_n, and thus CO_2 demand, in determining the leaf CO_2 supply to demand status over diurnal time courses.

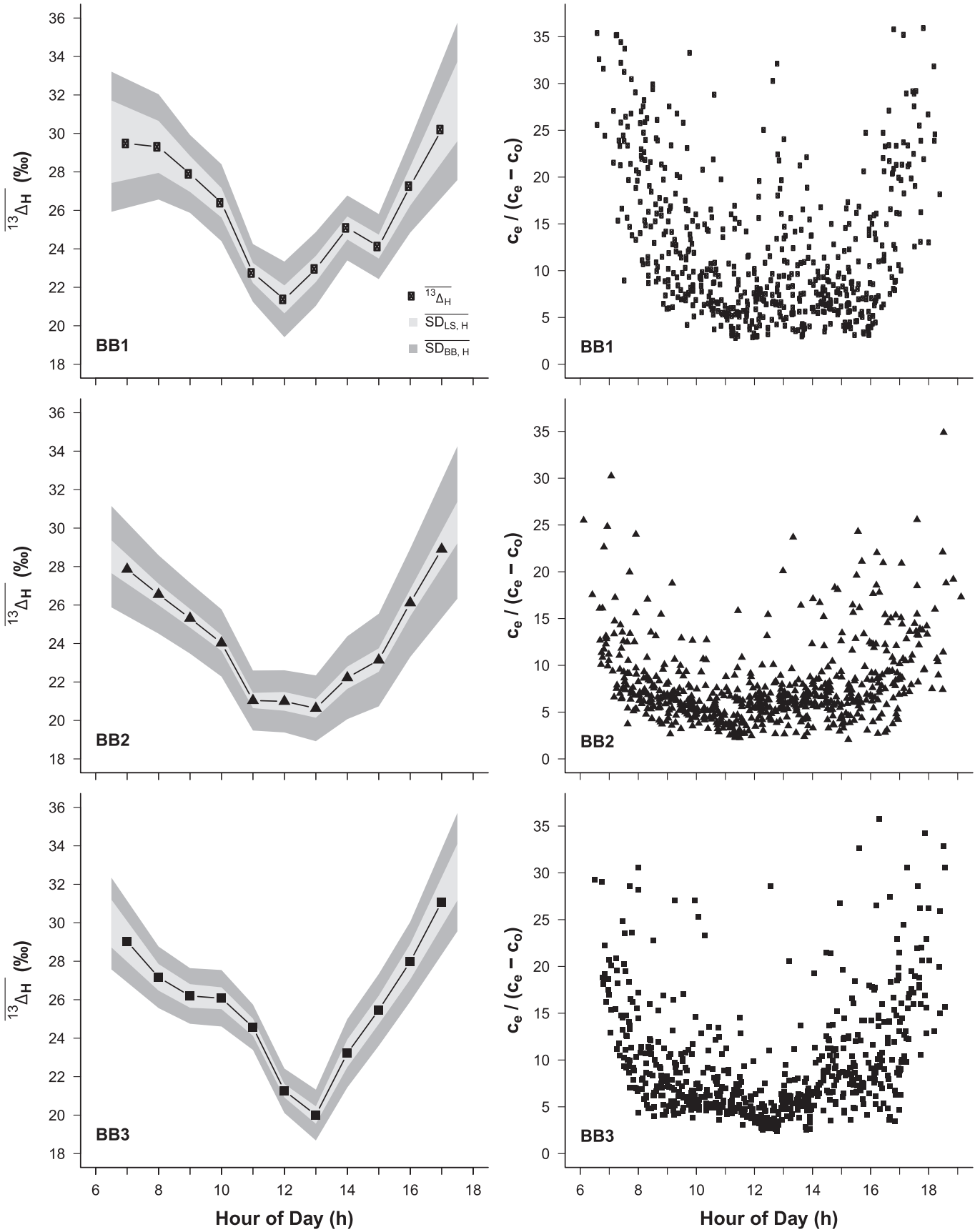

Fig. 3. Left: hourly means over the entire 2010 campaign of photosynthetic ^{13}C discrimination (symbols) and their associated propagated standard deviations for the three branch bags (BB1–BB3). Total standard deviation (SD_{BB}) and the standard deviation based solely on QCLAS-ISO measurement precision (SD_{LS}) are distinguished by darker and lighter shades of grey. Right: diurnal time courses of the factor $\xi = c_e/(c_e - c_o)$ for each branch bag, a good proxy for SD_{BB} (see Supplementary Fig. S6 available at *JXB* online).

Table 4. *Estimated contribution of twig CO_2 efflux (F_{twig}) to A_n during the 2010 field campaign, and relevant data used for the estimation of F_{twig} for three branch bags (BB1–BB3)*

F_{twig} was calculated per m^2 bark surface area. The contribution of F_{twig} to A_n was calculated per m^2 leaf surface area. Reported highest F_{twig} were observed under dark conditions only.

	Leaf surface area (m^2)	Bark surface area (m^2)	Bark/leaf ratio	Highest observed F_{twig} (μmol m^{-2} s^{-1})	Estimated contribution of F_{twig} to A_n (μmol m^{-2} s^{-1})
BB1	0.20	0.024	0.12	0.56	<0.07
BB2	0.32	0.025	0.08	0.63	<0.05
BB3	0.26	0.016	0.06	0.80	<0.05

Cumulated daily A_n (Fig. 6A) and PAR (Fig. 6D) likewise displayed a considerable predictive power for the day-to-day variability of $^{13}\Delta$ during the 2010 field campaign, that was substantially smaller during the 2009 field campaign (Fig. 6A, D).

In contrast, g_s displayed either no or little predictive power for $^{13}\Delta$ (Fig. 5, middle panel). Only BB1 in 2010 showed a linear relationship between $^{13}\Delta$ and g_s with an r^2>0.1, that was negative and thus covariant with A_n. In addition, mean daily g_s did not show predictive power for the day-to-day variability of $^{13}\Delta$ for any of the two field campaigns (Fig. 6B). Nonetheless, an increased instantaneous stomatal control, resulting in an instantaneous decrease of $^{13}\Delta$, was apparent at high VPD >2.0 kPa, frequently encountered in BB2 and BB3 at midday in 2009, but not in 2010 (Fig. 4D). Indeed under low VPD, a strong linear relationship between leaf transpiration (E) and VPD (r^2 for BB1–BB3 in 2010: 0.90, 0.93, and 0.90; all P values <0.0001) was observed, indicating little stomatal control, but at VPD >2–2.5 kPa, E started to decrease in response to stomatal control (Supplementary Fig. S2 available at *JXB* online). Measurements with VPD >2.0 kPa during the 2009 field campaign are highlighted in red in Fig. 5. Regression analysis on these highlighted data subsets revealed significant positive relationships between individual measurements of $^{13}\Delta$ and g_s, with the r^2 for the more sun-adapted BB2 further increasing with higher VPD thresholds (e.g. r^2=0.16 if VPD >2.5 kPa). Additional observations further suggested a gradual increase in stomatal control over several days during August 2009 that could not be explained by the above-mentioned instantaneous g_s response to high VPD but rather in response to soil water limitations. First, both midday g_s and early morning and late afternoon g_s displayed a successive and parallel day-to-day decrease during August 2009 (Fig. 4C), reflected in the concurrent decrease of instantaneous $^{13}\Delta$. Interestingly, the diurnal amplitude of $^{13}\Delta$ stayed approximately constant over that period (Supplementary Fig. S4 available at *JXB* online). Secondly, slopes of the linear sections (VPD <2.0 kPa) of the E to VPD regressions reduced by 33% for BB2 and by 43% for BB3 in 2009 compared with 2010 (Supplementary Fig. S2 available at *JXB* online). As a consequence, when only data from August 2009 were used (from day 225 to day 243), significant positive relationships between flux-weighted daily means of $^{13}\Delta$ and mean daily g_s were found (BB2, r^2=0.25, P<0.05, BB3, r^2=0.31, P<0.05; data not shown).

For the majority of the measurements, $^{13}\Delta$ exhibited the expected positive relationship with c_i/c_a (Fig. 5, right panel), however displaying r^2 usually lower than that of the regressions with A_n only. The relationship between $^{13}\Delta$ and c_i/c_a was also clearly not linear, hence lowering the predictive power of the regressions. The relationship between flux-weighted daily means of $^{13}\Delta$ and of c_i/c_a was also not significant for the individual campaigns, but started to become more significant when data from both years were included for the regression (Fig. 6C), or for individual branches (BB3) when only the August 2009 soil drying period was selected (not shown). Most importantly, $^{13}\Delta$ tended to be higher in 2010 than in 2009 for a given A_n/g_s (Fig. 6C). This offset could only be explained by differences in soil moisture between the two field campaigns (Fig. 6F), rather than differences in c_i/c_a (Fig. 6C).

Discussion

Reported variability of $^{13}\Delta$ under field conditions

Variations of flux-weighted daily means of $^{13}\Delta$ (9‰ in 2009 and 11‰ in 2010, Fig. 4A) were comparable with the mean diurnal variability of $^{13}\Delta$ (~9‰, Fig. 2K, L). High diurnal variabilities of $^{13}\Delta$ have been reported in previous field studies for other tree species, including (maximum diurnal amplitudes are given in parentheses): *Piper aduncum* (L.) (~40‰, Harwood *et al.*, 1998), *Picea sitchensis* (Bong., Carr) (~25‰, Wingate *et al.*, 2007), *Juniperus monosperma* (Engelm., Sarg.) (~35‰ and 15‰, respectively, Bickford *et al.*, 2009, 2010), and *P. pinaster* (~25‰, Wingate *et al.*, 2010). Absolute $^{13}\Delta$ values (Table 2) were likewise within the previously reported range. The characteristic diurnal pattern was also observed by Wingate *et al.* (2007, 2010), whereas Harwood *et al.* (1998) and Bickford *et al.* (2009, 2010) reported different, more variable diurnal time courses. Continuous seasonal on-line measurements of $^{13}\Delta$ have so far only been conducted by Wingate *et al.* (2010), who found a comparable 12‰ range for flux-weighted daily means of $^{13}\Delta$, and with 9‰ and 36‰ comparable minimum and maximum values for individual measurements of $^{13}\Delta$.

Plausibility of the diurnal $^{13}\Delta$ pattern

The assessment of $^{13}\Delta$ measurement uncertainty (Fig. 3) clearly demonstrated the plausibility of the diurnal $^{13}\Delta$ pattern, despite commonly smaller CO_2 drawdowns during early

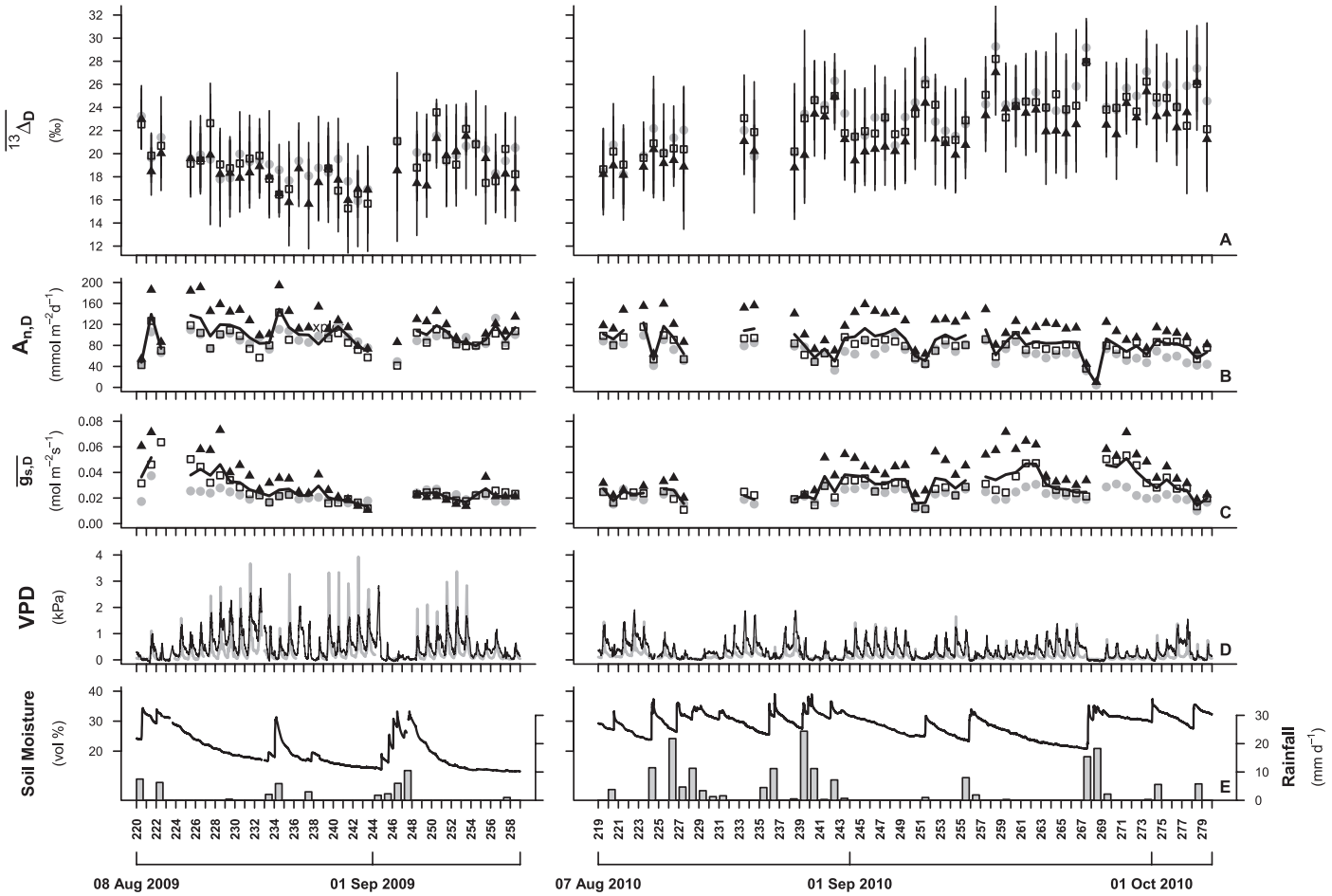

Fig. 4. Day-to-day variations of photosynthetic ^{13}C discrimination, gas exchange, microclimate, and site environmental variables during the 2009 and 2010 field campaigns. Measurements from the three branch bags are distinguished by different symbols. The time axis unit is day of year, with tick marks set at midnight. (A) Flux-weighted daily mean of photosynthetic ^{13}C discrimination, with their associated standard deviation; (B) cumulated daily net CO_2 assimilation; (C) daily mean of stomatal conductance for CO_2; (D) air vapour pressure deficit inside (grey line) and outside (black line) of BB3; and (E) soil moisture at 5 cm depth and daily rain amount at the site. Solid black lines in (B) and (C) represent the means of three branch bags. PAR and air temperature data are shown in Supplementary Fig. S5 available at *JXB* online.

morning and late afternoon measurements. A diurnal $^{13}\Delta$ pattern may likewise be expected outside the branch bags, despite certain chamber effects. Indeed, the expected plant physiological response to lower CO_2 mixing ratios experienced inside the branch bags (lower A_n and higher g_s) would lead to smaller, not larger, diurnal $^{13}\Delta$ amplitudes (Equation 1). The large $^{13}\Delta$ amplitude was further no artefact of high VPD gradients (lower g_s), as branch bag and ambient VPD resembled each other in 2010 (Fig. 4D). A persistence of the diurnal $^{13}\Delta$ pattern is also expected for upper canopy branches (Wingate *et al.*, 2010), as high photosynthetic capacities (Montpied *et al.*, 2009) and thus high CO_2 demand as well as a more stringent g_s regulation are likely to cause large c_i/c_a gradients.

Contribution of twig CO_2 efflux to total A_n

For the time of the year, the estimates of twig CO_2 efflux agreed well with other studies on beech for twigs of similar diameters (Damesin *et al.*, 2002; Damesin, 2003). Nonetheless, twig CO_2 efflux could have been two to three times as high, if measurements had been conducted earlier in the vegetation period instead of in August/September (Ceschia *et al.*, 2002; Damesin *et al.*, 2002; Damesin, 2003; Kuptz *et al.*, 2011). At the same time, the enclosure of several older twig age classes, along the axis of the ~80 cm long branch, probably kept twig CO_2 efflux rather small (Ceschia *et al.*, 2002; Wittmann and Pfanz, 2008). The observed diel cycle and the light-induced reduction of twig CO_2 efflux were most probably caused by CO_2 refixation by bark photosynthesis (e.g. Wittmann *et al.*, 2006; Berveiller *et al.*, 2007; Wittmann and Pfanz, 2008). Overall, the contribution of twig CO_2 efflux to A_n was probably only important under low light conditions, as generally found during early morning and late afternoon (Fig. 2A, B), thereby decreasing A_n by ~5–10% (Tables 2, 4).

Relationships of $^{13}\Delta$ to A_n and g_s reported in other studies

High prediction powers of A_n for the variability of $^{13}\Delta$ observed under or modelled for field conditions have also been reported in other studies. Bickford *et al.* (2009, 2010) also found higher prediction powers for, largely negative, $^{13}\Delta$

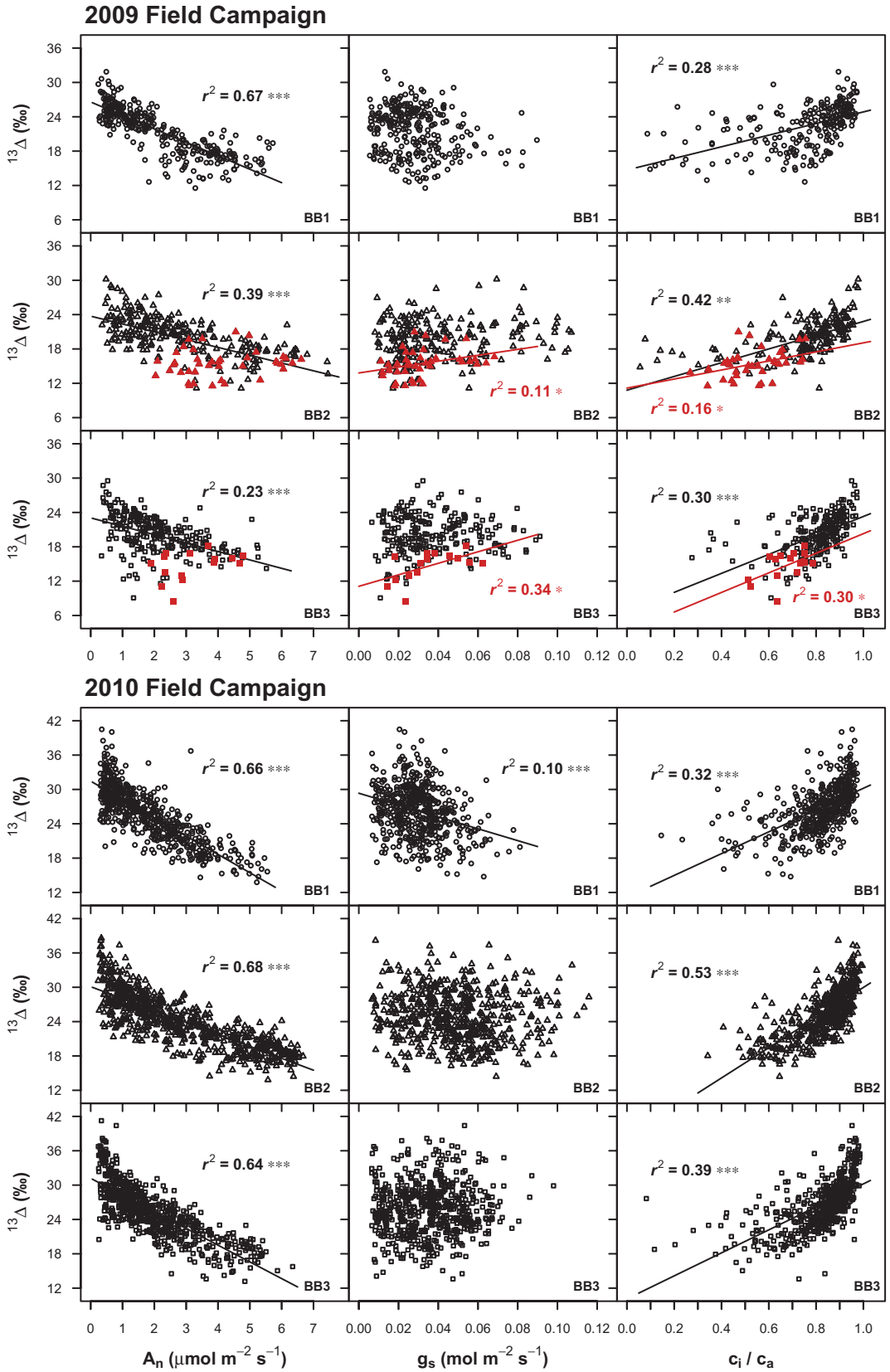

Fig. 5. Relationships between photosynthetic ^{13}C discrimination and net CO_2 assimilation (left panel), stomatal conductance for CO_2 (middle panel), and the c_i/c_a ratio (right panel) for the three branch bags (BB1–BB3) during the 2009 and 2010 field campaigns. Only significant regressions with $r^2 \geq 0.10$ are shown. Entire campaign r^2 are given in black. Observations with an air vapour pressure deficit >2.0 kPa inside the branch bags are distinguished with red, solid symbols. ***P<0.001; *P<0.05 for a given r^2.

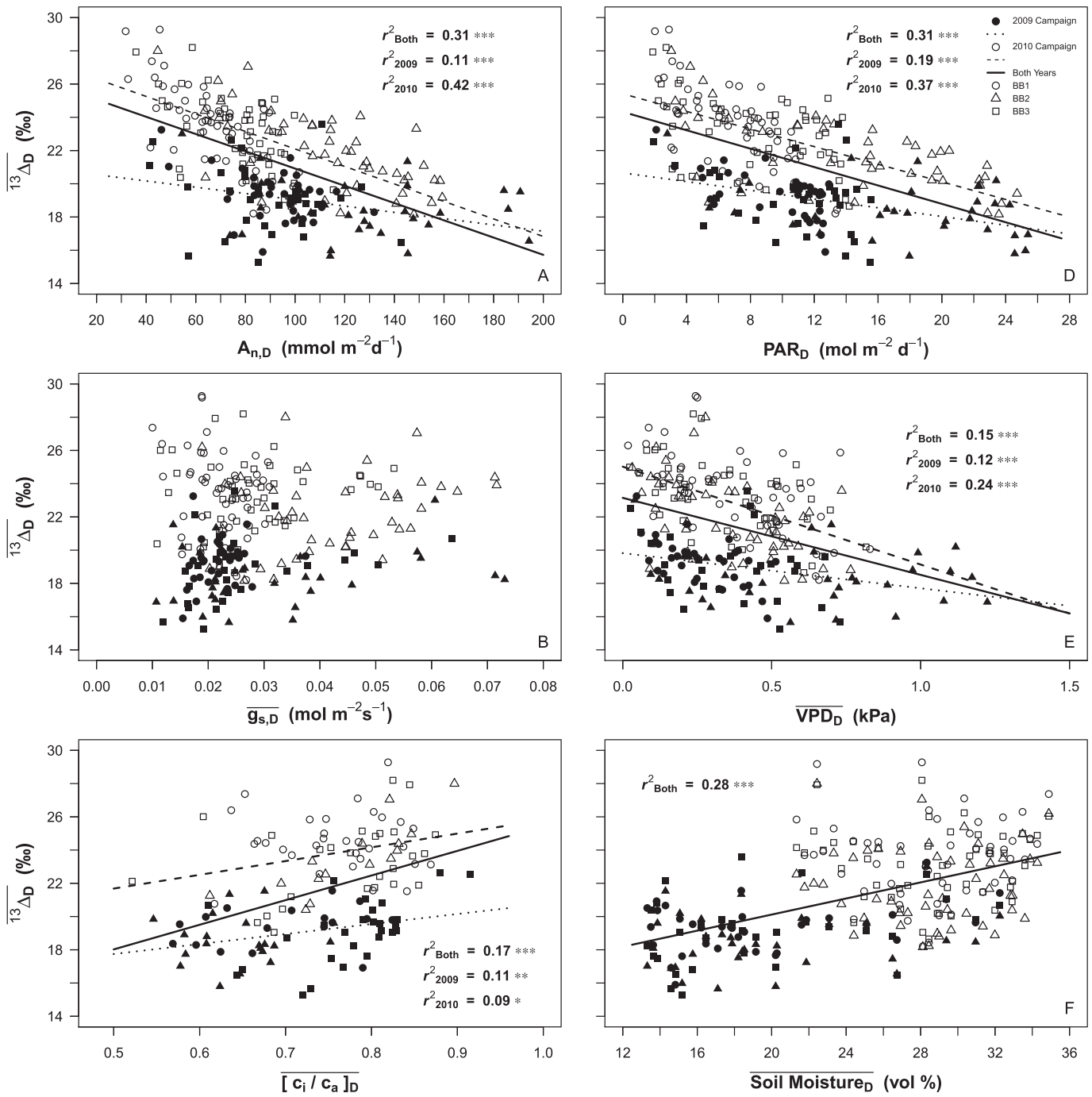

Fig. 6. Relationships between flux-weighted daily means of photosynthetic ^{13}C discrimination and (A) cumulated daily net CO_2 assimilation, (B) daily means of stomatal conductance for CO_2, (C) flux-weighted daily means of the c_i/c_a ratio, (D) cumulated daily photosynthetic active radiation, (E) daily means of air vapour pressure deficit within the branch bags, or (F) daily means of soil moisture at 5 cm depth. Regression included all values for one or both field campaigns. No differentiation between branch bags was made. Only significant regressions with $r^2 \geq 0.10$ are shown, with ***$P<0.001$, **$P<0.01$, and *$P<0.05$, respectively.

to A_n relationships than for, slightly positive or highly variable, $^{13}\Delta$ to g_s relationships. The observations from the present study further agree with predictions of canopy process models regarding the sensitivity of forest canopy $^{13}\Delta$ to gas exchange and environmental variables. For a temperate coniferous forest, Aranibar *et al.* (2006) implicitly predicted negative relationships between flux-weighted daily means of canopy $^{13}\Delta$ and incident radiation as well as VPD, comparable with those found here (Fig. 6D, E). However, their modelled canopy $^{13}\Delta$ correlated better with modelled stomatal conductance than with gross photosynthesis over the growing season. Baldocchi and Bowling (2003) predicted a negative, slightly curved relationship between canopy $^{13}\Delta$ and PAR (Supplementary Fig. S2 available at *JXB* online) for a deciduous forest, and remarked on its consistency with light response curves of forest canopy photosynthesis.

Driving mechanism of $^{13}\Delta$ variability on diurnal time scales

For diurnal time scales, g_s generally varied within a relatively smaller range of values than A_n (Fig. 2) and often exhibited no defined responses to potential environmental drivers (Supplementary Fig. S3 available at *JXB* online). These observations might indicate a more conservative diurnal or short-term regulation of g_s compared with A_n, except when VPD was >2.0 kPa (Fig. 5). Such putative regulatory differences between A_n and g_s, for example in the form of different response times to environmental drivers, might explain the observed large diurnal amplitudes of $^{13}\Delta$ (Fig. 2K, L). Indeed, a pronounced diurnal time course of PAR is likely to induce a pronounced diurnal time course of CO_2 demand, or A_n, that is not counteracted by equally large CO_2 supply, or g_s. Diurnal time courses of the resulting gradients between leaf and ambient CO_2 partial pressures (represented by c_i/c_a), reflected in $^{13}\Delta$ (Equation 1), are then consequently more strongly related to the diurnal variability of A_n than to that of g_s. This mechanism would explain the observed discrepancy between A_n and g_s in terms of predictive power for the variability of instantaneous $^{13}\Delta$ (Fig. 5). The constancy of diurnal amplitude of $^{13}\Delta$ in 2009 (Table 2), despite evidence for a more stringent g_s control, further supported the proposed driving mechanism. Nonetheless, variabilities in mesophyll conductance (Flexas *et al.*, 2012), mitochondrial respiration (Werner and Gessler, 2011), and photorespiration (e.g. Lanigan *et al.*, 2008) also influence the variability of $^{13}\Delta$ (Farquhar *et al.*, 1982). For example, true or apparent fractionations associated with mitochondrial day respiration could have increased $^{13}\Delta$ at low light, while photorespiration could have decreased $^{13}\Delta$ at high light, often co-occurring with high temperatures, thus contributing to, but not causing, the high predictive powers of the $^{13}\Delta$ to A_n relationships (Fig. 5).

Driving mechanisms of $^{13}\Delta$ variability on day-to-day time scales

For the 2010 field campaign, the strong relationships between flux-weighted daily means of $^{13}\Delta$ and cumulated daily A_n (Fig. 6A) as well as cumulated daily PAR (Fig. 6D) suggested that the same, above-proposed, mechanism was principally driving both short-term (diurnal) and a considerable share of the long-term (day-to-day) variability of $^{13}\Delta$. A considerable share of the day-to-day variability of $^{13}\Delta$ in 2010 (Fig. 4A) might thus simply be explained by day-to-day changes in CO_2 demand (Fig. 4B). Nonetheless, the general lack of predictive power of mean daily g_s for flux-weighted daily means of $^{13}\Delta$ (Fig. 6B) could also have originated in a generally complex regulation of g_s.

During the soil drying event in August 2009 (Fig. 4D), the gradual decrease of g_s (Fig. 4C) was likely even to be the dominant driver of the day-to-day variability of $^{13}\Delta$ (Fig. 4A). The concurrent decrease in A_n, likely to be caused by that of g_s, in contrast attenuated the decrease of $^{13}\Delta$. High VPD, and thus branch microclimate, alone could not explain that g_s decrease. The gradual nature of the g_s decrease instead suggested a root-derived stomatal regulation to increasing water limitation at the site, that was likely to reflect a whole-tree response. Weak stomatal responses of BB1 during the 2009 campaign appeared to contradict this argument. However, BB1 measured the most shaded of the three branches (Figs 2A, 6D). Likewise in 2010, it displayed the smallest day-to-day variations for A_n and g_s (Fig. 4B, C), whereas those for $^{13}\Delta$ (Fig. 4A) were comparable with the other branch bags. This simply originated in a smaller, more shade-adapted, response range of leaf gas exchange for BB1, whereas the overall A_n/g_s regulations did not noticeably differ between the trees (Fig. 5). In this context, it is clear why the 50% decrease of mean daily g_s for BB1 (from 0.03 mol m^{-2} s^{-1} to 0.015 mol m^{-2} s^{-1}) from DOY 225 to DOY 243 in 2009 had an impact on $^{13}\Delta$ comparable with the considerably larger decreases for the other two branch bags (Fig. 4C).

Relationship of $^{13}\Delta$ to c_i/c_a

Given Equation 1, the impact of the A_n to g_s trade-off on $^{13}\Delta$ should be best explained by a linear relationship between $^{13}\Delta$ and c_i/c_a. Yet, the positive linear relationships with c_i/c_a found here (Fig. 5) were strongly driven by the diurnal variability of A_n, and the inclusion of g_s did not increase the predictive power for $^{13}\Delta$. Measurement precision problems for g_s cannot be entirely ruled out, as branch bag field measurements are generally afflicted by issues such as stomatal heterogeneity (Kueppers *et al.*, 1999), possible gradients in leaf temperature for ~200 leaves, as well as error propagations from small differences for inlet and outlet measurements. However, the well-defined display of day-to-day trends (Fig. 4C) and the VPD response (Fig. 5) for g_s suggested that robust relationships between individual measurements of $^{13}\Delta$ and g_s (Figs 5, 6B) would have been extractable if present. The offset in $^{13}\Delta$ for a given c_i/c_a between the two years (Fig. 6C) may have originated in an alteration of a further, unmeasured, variable. For instance, a relatively lower mesophyll conductance (Flexas *et al.*, 2012) during the 2009 than during the 2010 field campaign could have been a potential cause of the relatively lower $^{13}\Delta$ for a given c_i/c_a in 2009 compared with 2010.

Conclusion

The first continuous on-line field measurements of $^{13}\Delta$ on a deciduous tree species (*F. sylvatica*) revealed a substantial hourly variability of instantaneous $^{13}\Delta$ that was embedded in a recurring diurnal pattern with a mean diurnal amplitude of ~9‰. The plausibility of the diurnal $^{13}\Delta$ pattern was assured by analyses of diurnal signal-to-noise ratios. Favourable bark to leaf surface area ratios kept the influence of twig CO_2 efflux on A_n small. A regression-based analysis led to the opinion that regulation differences for A_n and g_s responses to environmental drivers were the likely reason for the diurnal $^{13}\Delta$ pattern, indicating that the pronounced diurnal time courses of CO_2 demand (represented by A_n) were

not counteracted by equally large CO_2 supplies (represented by g_s). Day-to-day variations of $^{13}\Delta$ displayed considerable ranges of 8‰ (2009) and 11‰ (2010). A comparative analysis of gas exchange and environmental drivers for the two field campaigns indicated that the day-to-day variability of $^{13}\Delta$ was predominantly controlled by CO_2 supply in 2009 and by CO_2 demand in 2010.

Supplementary data

Supplementary data are available at *JXB* online.

The Supplementary data consist of four parts. The first part contains the formula appendix. The second part contains additional figures. The third part contains additional Materials and methods. The fourth part presents Materials and methods, Results, and figures for the analysis of $\delta^{13}C$ and C/N ratios of bulk leaf material sampled at approximately weekly intervals during both field campaigns.

Acknowledgements

We thank EMPA for allowing us the use of the Lägeren NABEL station and for provision of meteorological data to the Grassland Sciences group, ETH Zurich. For field work and sample preparation, we thank all ETH apprentices and student assistants involved, especially Laura Spring and Daniela Cervenka. We thank Christof Ammann (Agroscope Reckenholz-Tänikon) for alluding to the paper of Pape *et al.* (2009). For IRMS and EA analysis, we thank Roland A. Werner and Annika Ackermann (Isolab of the Grassland Sciences group, ETH Zurich). We further thank the forester at the Lägeren, Philipp Vock, and all ETH workshops involved in branch bag assembly. This work was supported by a Marie Curie Excellence grant from the European Commission to AK (MEXT-CT-2006–042268) and benefited from a COST-SIBAE Short-term Scientific mission grant to LG (COST-STSM-ECOST-STSM-ES0806-280211-005035). The INRA (Institut national de la recherche agronomique) department EFPA (Écologie des forêts, prairies et milieux aquatiques) is acknowledged for funding the sabbatical of JO in Cambridge and the salary for LG that resulted in the finalization of this manuscript.

References

Ahrends HE, Brugger R, Stockli R, Schenk J, Michna P, Jeanneret F, Wanner H, Eugster W. 2008. Quantitative phenological observations of a mixed beech forest in northern Switzerland with digital photography. *Journal of Geophysical Research: Biogeosciences* **113,** G04004.

Alden CB, Miller JB, White JWC. 2010. Can bottom-up ocean CO_2 fluxes be reconciled with atmospheric ^{13}C observations? *Tellus Series B-Chemical and Physical Meteorology* **62,** 369–388.

Aranibar JN, Berry JA, Riley WJ, Pataki DE, Law BE, Ehleringer JR. 2006. Combining meteorology, eddy fluxes, isotope measurements, and modeling to understand environmental controls of carbon isotope discrimination at the canopy scale. *Global Change Biology* **12,** 710–730.

BAFU. 2010. *NABEL – Luftbelastung 2009. Messresultate des Nationalen Beobachtungsnetzes für Luftfremdstoffe (NABEL). Umwelt-Zustand Nr. 1016*. Bern, Switzerland: Bundesamt für Umwelt (BAFU).

BAFU. 2011. *NABEL – Luftbelastung 2010. Messresultate des Nationalen Beobachtungsnetzes für Luftfremdstoffe (NABEL). Umwelt-Zustand Nr. 1118*. Bern, Switzerland: Bundesamt für Umwelt (BAFU).

Baldocchi DD, Bowling DR. 2003. Modelling the discrimination of $^{13}CO_2$ above and within a temperate broad-leaved forest canopy on houly to seasonal time scales. *Plant, Cell and Environment* **26,** 231–244.

Ballantyne AP, Miller JB, Baker IT, Tans PP, White JWC. 2011. Novel applications of carbon isotopes in atmospheric CO_2: what can atmospheric measurements teach us about processes in the biosphere? *Biogeosciences* **8,** 3093–3106.

Barbour MM, Farquhar GD. 2000. Relative humidity- and ABA-induced variation in carbon and oxygen isotope ratios of cotton leaves. *Plant, Cell and Environment* **23,** 473–485.

Barbour MM, Tcherkez G, Bickford CP, Mauve C, Lamothe M, Sinton S, Brown H. 2011. $\delta^{13}C$ of leaf-respired CO_2 reflects intrinsic water-use efficiency in barley. *Plant, Cell and Environment* **34,** 792–799.

Berveiller D, Kierzkowski D, Damesin C. 2007. Interspecific variability of stem photosynthesis among tree species. *Tree Physiology* **27,** 53–61.

Bickford CP, Hanson DT, McDowell NG. 2010. Influence of diurnal variation in mesophyll conductance on modelled ^{13}C discrimination: results from a field study. *Journal of Experimental Botany* **61,** 3223–3233.

Bickford CP, McDowell NG, Erhardt EB, Hanson DT. 2009. High-frequency field measurements of diurnal carbon isotope discrimination and internal conductance in a semi-arid species, *Juniperus monosperma*. *Plant, Cell and Environment* **32,** 796–810.

Bowling DR, Tans PP, Monson RK. 2001. Partitioning net ecosystem carbon exchange with isotopic fluxes of CO_2. *Global Change Biology* **7,** 127–145.

Brugnoli E, Farquhar GD. 2000. Photosynthetic fractionation of carbon isotopes. In: Leegood RC, Sharkey TD, von Caemmerer S, eds. *Photosynthesis: physiology and metabolism, Vol. 9*. Berlin: Springer, 399–434.

Cai T, Flanagan LB, Jassal RS, Black TA. 2008. Modelling environmental controls on ecosystem photosynthesis and the carbon isotope composition of ecosystem-respired CO_2 in a coastal Douglas-fir forest. *Plant, Cell and Environment* **31,** 435–453.

Cernusak LA, Ubierna N, Winter K, Holtum JAM, Marshall JD, Farquhar GD. 2013. Environmental and physiological determinants of carbon isotope discrimination in terrestrial plants. *New Phytologist* **200,** 950–965.

Ceschia E, Damesin C, Lebaube S, Pontailler JY, Dufrene E. 2002. Spatial and seasonal variations in stem respiration of beech trees (*Fagus sylvatica*). *Annals of Forest Science* **59,** 801–812.

Chen B, Chen JM. 2007. Diurnal, seasonal and interannual variability of carbon isotope discrimination at the canopy level in response to environmental factors in a boreal forest ecosystem. *Plant, Cell and Environment* **30,** 1223–1239.

Ciais P, Tans PP, White JWC, Trolier M, Francey RJ, Berry JA, Randall DR, Sellers PJ, Collatz JG, Schimel DS. 1995. Partitioning of ocean and land uptake of CO_2 as inferred by $\delta^{13}C$ measurements from the NOAA climate monitoring and diagnostics laboratory global air sampling network. *Journal of Geophysical Research-Atmospheres* **10,** 5051–5070.

Damesin C. 2003. Respiration and photosynthesis characteristics of current-year stems of *Fagus sylvatica*: from the seasonal pattern to an annual balance. *New Phytologist* **158,** 465–475.

Damesin C, Ceschia E, Le Goff N, Ottorini JM, Dufrene E. 2002. Stem and branch respiration of beech: from tree measurements to estimations at the stand level. *New Phytologist* **153,** 159–172.

Etzold S, Buchmann N, Eugster W. 2010. Contribution of advection to the carbon budget measured by eddy covariance at a steep mountain slope forest in Switzerland. *Biogeosciences* **7,** 2461–2475.

Eugster W, Zeyer K, Zeeman M, Michna P, Zingg A, Buchmann N, Emmenegger L. 2007. Methodical study of nitrous oxide eddy covariance measurements using quantum cascade laser spectrometery over a Swiss forest. *Biogeosciences* **4,** 927–939.

Evans JR, Sharkey TD, Berry JA, Farquhar GD. 1986. Carbon isotope discrimination measured concurrently with gas exchange to investigate CO_2 diffusion in leaves of higher plants. *Australian Journal of Plant Physiology* **13,** 281–292.

Farquhar GD, Cernusak LA.. 2012. Ternary effects on the gas exchange of isotopologues of carbon dioxide. *Plant, Cell and Environment* **35,** 1221–1231.

Farquhar GD, Ehleringer JR, Hubick KT. 1989. Carbon isotope discrimination and photosynthesis. *Annual Review of Plant Physiology and Plant Molecular Biology* **40,** 503–537.

Farquhar GD, O'Leary MH, Berry JA. 1982. On the relationship between carbon isotope discrimination and the intercellular carbon dioxide concentration in leaves. *Australian Journal of Plant Physiology* **9,** 121–137.

Farquhar GD, Richards RA. 1984. Isotopic composition of plant carbon correlates with water-use efficiency of wheat genotypes. *Australian Journal of Plant Physiology* **11,** 539–552.

Flexas J, Barbour MM, Brendel O, *et al.* 2012. Mesophyll diffusion conductance to CO2: an unappreciated central player in photosynthesis. *Plant Science* **193–194,** 70–84.

Gentsch L, Hammerle A, Sturm P, Wingate L, Ogée J, Siegwolf R, Plüss P, Baur T, Buchmann N, Knohl A. 2014. Carbon isotope discrimination during branch photosynthesis of *Fagus sylvatica*: a Bayesian modelling approach. *Plant, Cell and Environment* (in press).

Harwood KG, Gillon JS, Griffiths H, Broadmeadow MSJ. 1998. Diurnal variation of $\Delta^{13}CO_2$, $\Delta C^{18}O^{16}O$ and evaporative site enrichment of $\delta H_2{}^{18}O$ in *Piper aduncum* under field conditions in Trinidad. *Plant, Cell and Environment* **21,** 269–283.

Hemming D, Yakir D, Ambus P, *et al*. 2005. Pan-European $\delta^{13}C$ values of air and organic matter from forest ecosystems. *Global Change Biology* **11,** 1065–1093.

Hubick K, Farquhar G. 1989. Carbon isotope discrimination and the ratio of carbon gained to water lost in barley cultivars. *Plant, Cell and Environment* **12,** 795–804.

Kaiser J. 2008. Reformulated ^{17}O correction of mass spectrometric stable isotope measurements in carbon dioxide and a critical appraisal of historic 'absolute' carbon and oxygen isotope ratios. *Geochimica et Cosmochimica Acta* **72,** 1312–1334.

Knohl A, Buchmann N. 2005. Partitioning the net CO_2 flux of a deciduous forest into respiration and assimilation using stable carbon isotopes. *Global Biogeochemical Cycles* **19,** GB4008.

Kueppers M, Heiland I, Schneider H, Neugebauer PJ. 1999. Light-flecks cause non-uniform stomatal opening: studies with special emphasis on *Fagus sylvatica* L. *Trees (Berlin)* **14,** 130–144.

Kuptz D, Matyssek R, Grams TEE. 2011. Seasonal dynamics in the stable carbon isotope composition ($\delta^{13}C$) from non-leafy branch, trunk and coarse root CO_2 efflux of adult deciduous (*Fagus sylvatica*) and evergreen (*Picea abies*) trees. *Plant, Cell and Environment* **34,** 363–373.

Lai CT, Ehleringer JR, Schauer AJ, Tans PP, Hollinger DY, Paw U KT, Munger JW, Wofsy SC. 2005. Canopy-scale $\delta^{13}C$ of photosynthetic and respiratory CO_2 fluxes: observations in forest biomes across the United States. *Global Change Biology* **11,** 633–643.

Lanigan GJ, Betson N, Griffiths H, Seibt U. 2008. Carbon isotope fractionation during photorespiration and carboxylation in *Senecio*. *Plant Physiology* **148,** 2013–2020.

McNevin DB, Badger MR, Whitney SM, von Caemmerer S, Tcherkez GGB, Farquhar GD. 2007. Differences in carbon isotope discrimination of three variants of d-ribulose-1,5-bisphosphate carboxylase/oxygenase reflect differences in their catalytic mechanisms. *Journal of Biological Chemistry* **282,** 36068–36076.

Montpied P, Granier A, Dreyer E. 2009. Seasonal time-course of gradients of photosynthetic capacity and mesophyll conductance to CO_2 across a beech (*Fagus sylvatica* L.) canopy. *Journal of Experimental Botany* **60,** 2407–2418.

Nelson DD, McManus JB, Herndon SC, Zahniser MS, Tuzson B, Emmenegger L. 2008. New method for isotopic ratio measurements of atmospheric carbon dioxide using a 4.3 μm pulsed quantum cascade laser. *Applied Physics B* **90,** 301–309.

Ogée J, Peylin P, Ciais P, Bariac T, Brunet Y, Berbigier P, Roche C, Richard P, Bardoux G, Bonnefond JM, 2003. Partitioning net ecosystem carbon exchange into net assimilation and respiration using $^{13}CO_2$ measurements: a cost-effective sampling strategy. *Global Biogeochemical Cycles* **17,** 1070.

Pape L, Ammann C, Nyfeler-Brunner A, Spirig C, Hens K, Meixner FX. 2009. An automated dynamic chamber system for surface exchange measurement of non-reactive and reactive trace gases of grassland ecosystems. *Biogeosciences* **6,** 405–429.

Ponton S, Flanagan LB, Alstad KP, Johnson BG, Morgenstern KAI, Kljun N, Black TA, Barr AG. 2006. Comparison of ecosystem water-use efficiency among Douglas-fir forest, aspen forest and grassland using eddy covariance and carbon isotope techniques. *Global Change Biology* **12,** 294–310.

Pumpanen J, Kolari P, Ilvesniemi H, *et al*. 2004. Comparison of different chamber techniques for measuring soil CO_2 efflux. *Agricultural and Forest Meteorology* **123,** 159–176.

R Development Core Team. 2009. *R: A language and environment for statistical computing*. Vienna, Austria: R Foundation for Statistical Computing.

Rayment MB. 2000. Closed chamber systems underestimate soil CO_2 efflux. *European Journal of Soil Science* **51,** 107–110.

Riveros-Iregui DA, Hu J, Burns SP, Bowling DR, Monson RK. 2011. An interannual assessment of the relationship between the stable carbon isotopic composition of ecosystem respiration and climate in a high-elevation subalpine forest. *Journal of Geophysical Research: Biogeosciences* **116,** G02005.

Scheidegger Y, Saurer M, Bahn M, Siegwolf R. 2000. Linking stable oxygen and carbon isotopes with stomatal conductance and photosynthetic capacity: a conceptual model. *Oecologia* **125,** 350–357.

Sturm P, Eugster W, Knohl A. 2012. Eddy covariance measurements of CO_2 isotopologues with a quantum cascade laser absorption spectrometer. *Agricultural and Forest Meteorology* **152,** 73–82.

Sturm P, Knohl A. 2010. Water vapor δ^2H and $\delta^{18}O$ measurements using off-axis integrated cavity output spectroscopy. *Atmospheric Measurement Techniques* **3,** 67–77.

Subke J-A, Ineson P. 2010. Tracing photosynthetic isotope discrimination from leaves to soil. *New Phytologist* **188,** 309–311.

Taylor JR. 1997. *An introduction to error analysis: the study of uncertainties in physical measurements*. Sausalito, CA: University Science Books.

Tazoe Y, von Caemmerer S, Estavillo GM, Evans JR. 2011. Using tunable diode laser spectroscopy to measure carbon isotope discrimination and mesophyll conductance to CO_2 diffusion dynamically at different CO_2 concentrations. *Plant. Cell and Environment* **34,** 580–591.

Teskey RO, Saveyn A, Steppe K, McGuire MA. 2008. Origin, fate and significance of CO_2 in tree stems. *New Phytologist* **177,** 17–32.

Tuzson B, Mohn J, Zeeman MJ, Werner RA, Eugster W, Zahniser MS, Nelson DD, McManus JB, Emmenegger L. 2008. High precision and continuous field measurements of $\delta^{13}C$ and $\delta^{18}O$ in carbon dioxide with a cryogen-free QCLAS. *Applied Physics B-Lasers and Optics* **92,** 451–458.

von Caemmerer S, Evans JR. 1991. Determination of the average partial pressure of carbon dioxide in chloroplasts from leaves of several C_3 plants. *Australian Journal of Plant Physiology* **18,** 287–306.

Warren CR, Adams MA. 2006. Internal conductance does not scale with photosynthetic capacity: implications for carbon isotope discrimination and the economics of water and nitrogen use in photosynthesis. *Plant, Cell and Environment* **29**. 192–201.

Werner C, Gessler A. 2011. Diel variations in the carbon isotope composition of respired CO_2 and associated carbon sources: a review of dynamics and mechanisms. *Biogeosciences* **8,** 2437–2459.

Wingate L, Ogée J, Burlett R, Bosc A, Devaux M, Grace J, Loustau D, Gessler A. 2010. Photosynthetic carbon isotope discrimination and its relationship to the carbon isotope signals of stem, soil and ecosystem respiration. *New Phytologist* **188,** 576–589.

Wingate L, Seibt U, Moncrieff JB, Jarvis PG, Lloyd JON. 2007. Variations in ^{13}C discrimination during CO_2 exchange by *Picea sitchensis* branches in the field. *Plant, Cell and Environment* **30,** 600–616.

Wittmann C, Pfanz H. 2008. General trait relationships in stems: a study on the performance and interrelationships of several functional and structural parameters involved in corticular photosynthesis. *Physiologia Plantarum* **134,** 636–648.

Wittmann C, Pfanz H, Loreto F, Centritto M, Pietrini F, Alessio G. 2006. Stem CO_2 release under illumination: corticular photosynthesis, photorespiration or inhibition of mitochondrial respiration? *Plant, Cell and Environment* **29,** 1149–1158.

Yakir D, Wang XF. 1996. Fluxes of CO_2 and water between terrestrial vegetation and the atmosphere estimated from isotope measurements. *Nature* **380,** 515–517.

Yakir D. 2003. The stable isotopic composition of atmospheric CO_2. In: Holland HD, Turekian KK, eds. *Treatise on geochemistry*. Oxford: Pergamon, 175–212.

Zhang J, Griffis TJ, Baker JM. 2006. Using continuous stable isotope measurements to partition net ecosystem CO_2 exchange. *Plant, Cell and Environment* **29,** 483–496.

Zobitz JM, Burns SP, Reichstein M, Bowling DR. 2008. Partitioning net ecosystem carbon exchange and the carbon isotopic disequilibrium in a subalpine forest. *Global Change Biology* **14,** 1785–1800.